Quantitative study of C—H bonding in polymerlike amorphous carbon films using *in situ* infrared ellipsometry

T. Heitz,* B. Drévillon, C. Godet, and J. E. Bourée
Laboratoire de Physique des Interfaces et des Couches Minces (UMR 7647 CNRS), Ecole Polytechnique, 91128 Palaiseau Cedex, France
(Received 15 April 1998)

Polymerlike hydrogenated amorphous carbon (a-C:H) films have been deposited by plasma CVD at low temperature and low pressure. Vibrational properties have been investigated by *in situ* infrared ellipsometry as a function of film thickness. Hydrogen distribution within the films has been changed by varying the ion energy impinging on the film surface. Vibrational properties of C—H stretching and bending modes have been analyzed as function of self-bias (V_{bias}) in terms of frequency, bandwidth, and intensity. Absorption strengths are associated with effective charges that have been calculated for the different sp^3 CH_n groups. In order to make a comparison with values of organic chemistry, a general review of infrared spectra including alkanes, alkenes, and aromatic hydrocarbons is presented. A dipole description taking into account the local environment of CH bonds is developed showing that methyl and methylene group effective charges are similar for polymeric a-C:H and C_xH_y organic compounds. Line broadening and frequency shift effects are found to depend on the type of CH groups and are explained through a model including strain and dipole-dipole interactions. The sensitivity of effective charges to the local environment and the determination of CH_n group densities are used to propose a description of the hydrogenated network structure. [S0163-1829(98)01044-3]

I. INTRODUCTION

Hydrogenated amorphous carbon (a-C:H) films show remarkable physical and chemical properties such as high hardness, electrical resistivity, and near-infrared (IR) transparency or room-temperature luminescence.[1,2] These properties are closely related to the film microstructure, depending on the hybridization state of carbon atoms (sp^2 or sp^3) and on hydrogen distribution among these two configurations. Several techniques have been used to investigate hydrogen content and the sp^2/sp^3 ratio, such as nuclear magnetic resonance[3] (NMR), electron energy loss spectroscopy[4] (EELS), and infrared absorption spectroscopy[5,6] (IRAS). The first technique can provide quantitative results on the sp^2/sp^3 ratio but needs a large amount of material; the second one yields inconsistent conclusions in the low-energy range (0–40 eV).[4] IRAS is a widespread technique but faces many problems for providing quantitative results, arising from IR oscillator strength changes and band overlapping.

Using IRAS technique, some authors[7–9] have tried to determine the total H content by calculating the whole absorption area of the stretching (around 2950 cm^{-1}) or bending (around 1450 cm^{-1}) bands. However, the results were inconsistent with other direct techniques like elastic recoil detection (ERD). The decrease of the IRAS signal observed with increasing sp^2/sp^3 ratio had then been interpreted in terms of bound (IR active) and unbound (IR inactive) hydrogen[8,9] leading to the conclusion that up to 50% of hydrogen can be trapped as H_2 molecules. Nevertheless, inelastic neutron scattering has shown that the H_2 fraction[10] contributing to the total hydrogen content is low. This contradiction comes from the hypothesis of constant IR absorption strengths that had often been assumed[6,7,11,12] to facilitate IR data analysis. Jacob[13] has shown that the procedure used by Brodsky[14] in the case of amorphous hydrogenated silicon (a-Si:H) to calculate H concentration from IR data, cannot be applied to a-C:H owing to changing absorption strengths. Furthermore, as hydrogen is not equally distributed between the sp^2 and sp^3 phases, and as no quantitative data on the transition moments have been so far available, the evaluation of the sp^2/sp^3 ratio by IRAS leads systematically to high values, compared with NMR data:[15] IR results have thus to be corrected by empirical factors to be in agreement with NMR results.[15]

In order to check hydrogen distribution, fitting procedures using Lorentzian or Gaussian shapes are necessary to get the vibrational contribution of each group since the different CH_n bands overlap. Nevertheless decomposition has to be cautiously performed so that results do not depend on the choice of the number of bands as well as on the free parameters selected for each band (width, frequency). Finally, no quantitative conclusions can be drawn about hydrogen distribution and film microstructure from a band decomposition unless the absorption strengths for each CH_n unit are known.

Previous IR analyses[16,17] have revealed that, in the field of organic compounds, some transition dipole moments can be considered as a constant. The aim of this paper is, in particular, to check whether this assumption is valid in the case of polymerlike a-C:H films. The experimental deposition setup described in Sec. II allows to obtain a large range of polymeric carbon films having different sp^2/sp^3 ratios. In Sec. III, the general formalism of IR absorption is presented in terms of effective charges and local field corrections. In order to perform reliable calculations, a specific method, which will be presented in Sec. IV, is used to analyse a-C:H film vibrational properties. This procedure is partially based on the method used by Shanks *et al.*[18] and Langford *et al.*[19] for a-Si:H thin films: transition dipole moments are calculated by combining absorption intensity measurements and deter-

 ©1998 The American Physical Society

mination of the total hydrogen amount measured independently. In the case of *a*-C:H films, the procedure used by Shanks and Langford cannot be directly applied since many vibrational bands overlap and since the number of CH_n vibrational bands is very high. In order to get a reliable determination of effective charges, our method takes advantage of IR measurements for different vibrational modes as a function of thickness, which represents a useful contribution in the way of analyzing *a*-C:H film IR properties.

Among IR spectroscopic techniques, *in situ* IR ellipsometry (IRSE) has been chosen for its high sensitivity[20] and for its capability to follow film growth.[21] Moreover, vibrational peaks, no longer identified by extrema as in classical IR transmission experiments but by inflections, can be mostly directly observed in spectra, which facilitates band decomposition. To compare vibrational properties of hydrocarbons and *a*-C:H films, IR absorption strengths of CH_n units in organic compounds have been reviewed in detail and are reported in Sec. V. The results of our global analyzis are presented in Sec. VI. Each vibration is analyzed in terms of frequency, band width, and intensity. Effective charge ratios are determined for sp^3 CH_3 and CH_2 groups in both bending and stretching modes. Using ERD measurements, sp^3 CH effective charge is found as a function of self-bias, which represents the electrical potential difference between the plasma and the substrate holder. Hydrogen bonding in the sp^2 phase is determined through the analysis of sp^2 CH_n vibrations in both bending and stretching modes. All the results are interpreted by taking into account the C—H bond local environment and the internal strain effects. Finally, this global analysis provides some guidelines for a microstructural representation of *a*-C:H.

II. EXPERIMENTAL DETAILS

a-C:H films are deposited at a low-temperature (70 °C) and low-pressure (300 mTorr) by a double plasma radio-frequency (RF)/microwave (MW) technique.[22] MW plasma is formed in a quartz tube where a mixture of hydrogen and argon is introduced. Butane is directly injected near the substrate holder where a RF discharge is created. In order to increase the signal/noise ratio of IR measurements, *a*-C:H films were deposited on metallic substrates. A 1500-Å-thick palladium (Pd) layer was evaporated on *c*-Si and, for a better adhesion of carbon films, was exposed *in situ* to a silane flow at 280 °C. As a consequence of this treatment, a $PdSi_x$ alloy is formed[23] at the substrate surface promoting a good adhesion of carbon films, even at high RF power. UV-visible ellipsometry measurements have shown that this treated Pd can still be optically considered as a metallic substrate. As vibrational and optical film properties are essentially determined by RF power,[24] *a*-C:H films are deposited using an increasing self-bias voltage (V_{bias}), which allows us to obtain a large range of materials, from transparent polymer to more absorbing carbon layers. Film density is obtained by combining Rutherford backscattering (RBS) and UV-visible ellipsometry measurements. Hydrogen concentration, which is determined through ERD analysis, is found to vary from 53 to 40 at. %. UV-visible optical properties of such films have been reported elsewhere.[25] Let us mention that the Forouhi-Bloomer[26] optical gap of the deposited *a*-C:H films is related to the sp^2 content[27] and decreases from 3 eV ($V_{\text{bias}}=-20$ V) to 1 eV ($V_{\text{bias}}=-200$ V).

Vibrational properties are investigated as a function of film thickness by *in situ* IR ellipsometry. The entire spectral range (1000–4000 cm^{-1}) is studied using a $Hg_xCd_{1-x}Te$ detector. To get a better sensitivity, the particular C—H stretching region near 3000 cm^{-1} is also analyzed using an InSb detector. IR properties are determined through the analysis of (ψ,Δ) spectra defined by

$$\frac{r_p}{r_s}=\tan\,\psi e^{i\Delta}, \tag{1}$$

where r_p and r_s are the reflection coefficients for *p*- and *s*-polarized light. For a given thickness, spectra are accumulated 1000 times with a step of 4 cm^{-1} so that the sensitivity on (ψ,Δ) is (0.1°,0.03°). IR analysis is performed using the complex ellipsometric density *D* (Ref. 28) defined by

$$D=[\ln\tan(\psi_s)-\ln\tan(\psi)]+i(\Delta_s-\Delta), \tag{2}$$

where (ψ_s,Δ_s) corresponds to the substrate. In case of thin films deposited on metallic substrates, *D* can be expressed using a first-order expansion on σd:

$$D=4i\pi\,\sin\,\theta_0\,\tan\,\theta_0\left(1-\frac{1}{\varepsilon_f}\right)d\sigma, \tag{3}$$

where *d* is the film thickness and σ the wave number; θ_0 is the incidence angle and ε_f the dielectric function of the film. As CH bands are weak, *D* can be expressed as the sum of two separated terms, the first characterizing the transparency region, the other including vibration contributions:

$$D=4i\pi\,\sin\,\theta_0\,\tan\,\theta_0\left[\left(1-\frac{1}{\varepsilon_\infty}\right)d\sigma+\left(\frac{1}{\varepsilon_\infty^2}\sum_k\Delta\varepsilon_k\right)d\sigma\right]. \tag{4}$$

Outside vibrational bands, ε_f is considered as a constant equal to ε_∞. The contribution of the *k*th vibration to the whole dielectric function ($\Delta\varepsilon_k$) is modeled by a Lorentzian function,

$$\Delta\varepsilon_k=\frac{f\sigma_0^2}{\sigma_0^2-\sigma^2+i\Gamma\sigma}, \tag{5}$$

where σ_0 is the vibrational frequency (in cm^{-1}) and Γ a damping parameter (bandwidth). The coefficient *f* represents the transition dipole moment.

C—H bonding can be determined by investigating both the real and imaginary parts of *D* (Re *D* and Im *D*). However, in the present work, the analysis is focused on Im *D* for the following reasons. At first, (ψ,Δ) is calculated by combining fundamental (J_0), first (J_1), and second harmonic (J_2) of the IR signal. It could be shown[29] that ψ results from a combination of those three terms using two calibration parameters. The determination of Δ is simpler and more reliable since it only depends on the ratio J_2/J_1 and on one calibration parameter. As a consequence, the reproducibility and precision of Δ will be far better. Looking at Eq. (5), vibrations will be identified by extrema on Re *D* and by inflections on Im *D*. In the case of weak band (e.g., C—H), the vibration localization and identification are facilitated by

analyzing jumps rather than bumps. At last, Eq. (4) proves that one needs to calculate ε_∞ in order to perform quantitative measurements. In the first-order approximation, Re D will not depend on ε_∞ outside the bands. It is therefore impossible to properly analyze C—H bonding by using only Re D whereas a complete study can be achieved by investigating Im D spectra.

III. VIBRATIONAL ABSORPTION FORMALISM

Considering a distribution of dipoles embedded in a dielectric matrix, the general expression of the absorption properties associated with the jth vibrational transition is described by the parameter A_j:

$$A_j = \int_{\text{band}} \alpha(\omega) \frac{d\omega}{\omega}, \tag{6}$$

where α is the absorption coefficient and ω the frequency (in s^{-1}). In the case of dipoles in the gas phase, assuming the double harmonic approximation (i.e., dipole considered as a harmonic oscillator with an electric moment $\boldsymbol{\mu}$ depending linearly on the normal coordinate Q_j of the jth vibration), A_j can be expressed as

$$A_j = \frac{1}{12\varepsilon_0 c^2} \frac{Ng_j}{\omega_j} \left| \frac{\partial \boldsymbol{\mu}}{\partial Q_j} \right|^2, \tag{7}$$

where N is the dipole density, c the velocity of light in vacuum, ω_j the band center, and g_j the degeneracy of the mode. In the liquid or solid phase, owing to the mutual interactions of dipoles and to the dielectric properties of the medium, Eq. (7) becomes[30]

$$A_j = \frac{1}{12\varepsilon_0 c^2} \frac{Ng_j}{\omega_j} \left| \frac{\partial \boldsymbol{\mu}}{\partial Q_j} \right|^2 \frac{1}{n} f_{\text{int}}^2, \tag{8}$$

where the term f_{int} is equal to

$$f_{\text{int}} = \frac{E_i}{E}, \tag{9}$$

where E_i and E are, respectively, the internal (or local) field acting on the dipole and the macroscopic field in the dielectric of refractive index n. The two terms $|\partial \boldsymbol{\mu}/\partial Q_i|$ and f_{int} will be presented separately.

A. Internal field correction

The term f_{int} has been widely studied for molecules diluted in a solvent. Ratajczak[31] has shown that the change of intensity from gas to solution for a given band could be fairly explained in terms of the Lorentz internal field correction. If n is the refractive index of the solvent, f_{int} has the expression

$$f_{\text{int}} = \frac{(2+n^2)}{3}. \tag{10}$$

Onsager has demonstrated that this formula is a particular case of a more general expression where the long-range dipolar interactions are taken into account.[32] The Onsager field is the field inside a sphere of dielectric constant ε surrounded by a medium of dielectric constant ε_m. Cardona[33] and other authors[34] have successfully applied this model to the vibrational properties of a-Si:H, considering that Si—H dipoles are inside a spherical cavity ($\varepsilon = 1$) surrounded by an a-Si matrix. In that case, f_{int}, which corresponds to the Maxwell-Garnett correction, can be written as

$$f_{\text{int}} = \frac{3\varepsilon_m}{1+2\varepsilon_m}. \tag{11}$$

When the cavity is not spherical, the symmetry is broken so that f_{int} depends on the size of the cavity and on the vibrational mode.[18]

For a quantitative determination of the C—H oscillator density, f_{int} should be known. As our carbon films are H rich, each C—H dipole is surrounded by a hydrogenated carbon matrix: the Lorentz correction seems then to be better adapted in our case and will be considered for the calculations performed in the following sections. This assumption will be discussed in more detail in Sec. VII A.

B. Effective dynamical charge

In order to describe more physically vibrations and to find parameters transferable from one molecule to another, vibrational coordinates (R_t), which characterize the atom displacements, have been used. (R_t) can be separated into two subsets $\{r\}$ and $\{\phi\}$ for, respectively, stretching and bending components. In the equilibrium charges and charge flows (ECCF) (Ref. 35) model, at any instant, $\boldsymbol{\mu}$ is due to localized charges (q_k) on atoms so that

$$\boldsymbol{\mu} = \sum_{\text{atoms}} q_k r_k \mathbf{e}_k, \tag{12}$$

where $\mathbf{e}_k$ is the bond unit vector and r_k the internuclear distance. These parameters can be directly related to the bond moment dipole $\boldsymbol{\mu}_k$, generally used in the valence optical theory.[36] In the zero-order approximation, no interactions between bond moments are considered, which leads to the simple expression[37]

$$\frac{\partial \boldsymbol{\mu}_k}{\partial R_t} = \frac{\partial \boldsymbol{\mu}_k}{\partial R_k}. \tag{13}$$

The dipole moment variation produced during vibration is then directed along the bond in the stretching mode and perpendicular to the bond (along $\mathbf{e}_k^{\perp}$) in the bending mode:

$$\frac{\partial \boldsymbol{\mu}_k}{\partial r} = q_k^0 \mathbf{e}_k + r_k^0 \frac{\partial q_k}{\partial r_k} \mathbf{e}_k \quad \text{(stretching)}, \tag{14}$$

$$\frac{\partial \boldsymbol{\mu}_k}{\partial \phi} = q_k^0 r_k^0 \mathbf{e}_k^{\perp} \quad \text{(bending)}. \tag{15}$$

The zero indices characterize the equilibrium values. With such a description, many fundamental properties as intramolecular and intermolecular interactions or bond energies[38] can be deduced from IR data. In Table I, different equilibrium charges (q_H^0), bond lengths (r_H^0), and charge flows $(\partial q_H/\partial r_H)$ for a hydrogen atom attached to carbon in various configurations are given.[39] From Table I, it is evident that IR band intensities of C—H vibrations will depend on the hybridization states of both the α (first H neighbor) and β

TABLE I. Equilibrium bond lengths and charges, and charge flows on H atoms for different C—H configurations.

C—H configuration	r_H^0 (Å)	q_H^0 ($\|e\|$ unit)	$\frac{\partial q_H}{\partial r_H}$ ($\|e\|$Å^{-1})
—C—C—H	1.096	0.045	−0.21
═C—C—H	1.096	0.068	−0.21
═C—H	1.085	0.134	−0.22

(second H neighbor) C atoms, in agreement with experimental findings.[16,17] We can also notice that A_j^{ben} (bending mode) increases and A_j^{str} (stretching mode) decreases with increasing q_H^0.

However interesting the bond model theory is to analyze hydrocarbon IR spectra, Gribov has shown[36] that interaction terms of dipole moments of CH_2 or CH_3 groups can be as significant as one-bond terms so that Eq. (13) should be modified. Dipole moments of C—H bonds attached to the same carbon atom are indeed not purely additive. C—H absorption properties should thus no longer be described in terms of C—H bonds but as the result of different CH_n group vibrations. Band intensities of most C_xH_y compounds can be indeed fairly simulated[36,16,17] by assuming that different CH_n group vibrations do not interact with each other and by taking into account the local environment (first and second H neighbors) of CH_n units. Looking at Eqs. (14) and (15), the group movements can be described by a parameter e^* (in electron charge unit), which depends on the vibrational mode and symmetry, on the type of group (CH, CH_2, or CH_3), and on the local group environment (first and second neighbors). Using the harmonic approximation and considering the contribution of each vibration to the whole dielectric function, A_j can be expressed as[33]

$$A_j = \frac{\pi}{2c\varepsilon_0 n m \omega_j} N e^{*2} f_{\text{int}}^2, \tag{16}$$

where m will be taken as the reduced mass of the C—H bond. Comparing Eqs. (8) and (16), e^* is found to be proportional to $\sqrt{g_j}|\partial\boldsymbol{\mu}/\partial Q_i|$. The parameter e^* is generally

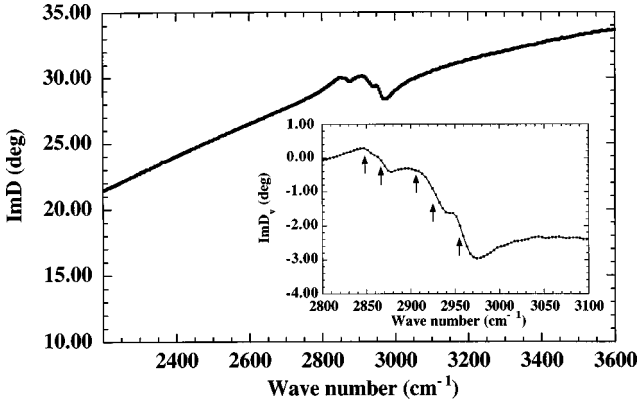

FIG. 1. a-C:H imaginary part (Im D) in degrees of the ellipsometric density. Inset is the subtraction of Im D with its linear wave number dependence. Vibrations are localized by negative inflections (arrows).

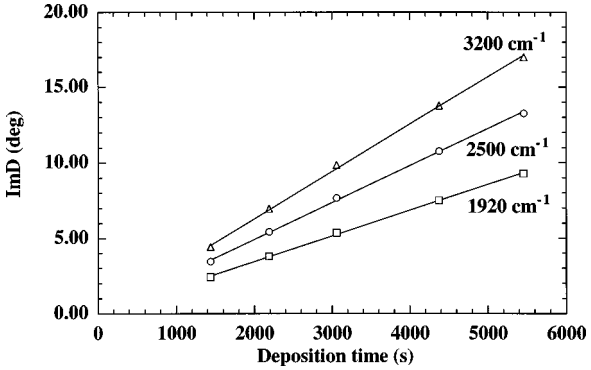

FIG. 2. Evolution of Im D vs deposition time for different wave numbers.

called the effective dynamical charge and has been widely used in the IR studies on hydrogenated amorphous silicon[33,34] (a-Si:H). Even if e^* is often considered as an empirical parameter in solid-state physics, it can be determined by *ab initio* calculations for quite simple molecules. In the present case, such calculations have not been performed: effective charges are only determined in this work from experimental results.

IV. DATA ANALYSIS

As previously reported, vibrational properties of a-C:H films have been studied by analyzing the imaginary part of the ellipsometric density. Figure 1 shows a typical Im D spectrum that can be divided into two parts, that is, inside or outside the vibrational bands. The shape of the latter region is a straight line the slope of which is related to ε_∞. Inside the bands, C—H bending and stretching vibrations are studied by subtracting Im D with its linear wave number dependence: the resulting density, Im D_v, shows negative inflections (see inset of Fig. 1) corresponding to the different CH_n group vibrations. More precisely, three steps are directly observed in the inserted figure. The vibrational study as a function of thickness (Sec. VI) and the analysis of hydrocarbon vibrational frequencies (Sec. V) will show that five vibrations (localized by arrows) are in fact involved in the stretching (2800–2970 cm^{-1}) region.

A. Out-of-band region analysis

According to Eq. (4), ε_∞ can be found through slope analysis of the imaginary part of D outside the bands. Figure

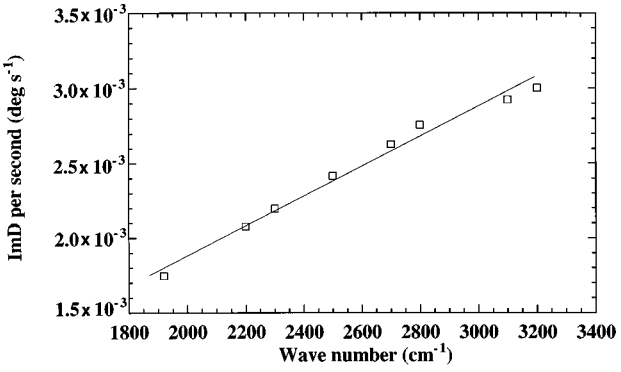

FIG. 3. Evolution of Im D per time unit vs wave number.

TABLE II. Frequencies of CH vibrations in bending mode.

Bending mode	Dischler[a]	Rao[b]	Bellamy[c]	Wexler[d]	Colthup[e]	This work
sp^3 CH_3 sym	1325	1375	1370/80	1379	1370/80	1370/80
sp^3 CH_3 asym	1490	1450/60	1440/70	1458/67	1440/70	1465
sp^3 CH_2	1450	1460/70	1455/70	1467	1445/75	1450
sp^2 CH_2	1450	1400/20	1410/20	1416	1400/20	1418
sp^2 CH olef.	1280	1400/20	1405	1404	1400/30	1404
sp^2 CH arom.	1445				1450	

[a]Reference 11.
[b]Reference 47.
[c]Reference 46.
[d]Reference 43.
[e]Reference 66.

2 confirms that the evolution of Im D versus deposition time is linear, whatever the wave number. In the whole detection area, the slopes, which are equal to Im D per time unit, are calculated and their dependence with wave number is shown in Fig. 3. The linear relationship is still consistent with Eq. (4), the proportionality coefficient p_1 having the expression

$$p_1 = 4\pi \sin\theta_0 \tan\theta_0 \left(1 - \frac{1}{\varepsilon_\infty}\right) R_d , \qquad (17)$$

where R_d is the deposition rate measured by UV-visible ellipsometry. Using this method ε_∞ is determined in the whole detection range with a precision of ± 0.3.

B. Vibration analysis

As can be seen in Tables II and III, in C–H bending and stretching regions, 5 to 9 bands can overlap, which makes the vibrational analysis particularly difficult. In order to separate each band, a decomposition is necessary but has to be carefully done in view of the high number of parameters. The contribution of the present work is, among others, to perform IR spectra decompositions as a function of film thickness. To the knowledge of the author, such an analysis has not been performed so far for a-C:H films. Their vibrational properties are generally determined[10,12] by using the decomposition of one spectrum corresponding to one given experimental measurement.

In the present case, for one given experimental condition, 5–8 spectra have been recorded *in situ* at different deposition times. At first, one tries to decompose Im D_v spectra by using the number of vibrations that can be directly observed by the eye and by taking into account the fact that an asymmetric vibration always goes together with a symmetric one. For example, in the case of Fig. 1, the first decomposition is made using four vibrations corresponding to sp^3 CH_2 and sp^3 CH_3 groups in symmetric and asymmetric modes. This kind of procedure is performed for all thicknesses. If the decompositions are not satisfactory, another vibration is added. The line position of this new vibration has to correspond to a specific CH_n group and must not depend on the film thickness. This procedure allows us, for example, to see evidence of the sp^3 CH stretching vibration (see Sec. VI and Fig. 15).

When the number of vibrations has been determined, decomposition of Im D_v is carried out so that frequencies and widths versus thickness stay constant within, respectively, 0.3 % and 15 %. The intensity ratio between symmetric and asymmetric modes cannot be assumed to be constant (see below). Examples of such decomposed spectra are presented

TABLE III. Frequencies of CH vibrations in stretching mode.

Stretching mode	Dischler[a]	Rao[b]	Bellamy[c]	Wexler[d]	Colthup[e]	This work
sp^3 CH_2 sym	2850	2853	2853	2855	2843/63	2845/60
sp^3 CH_3 sym	2875	2872	2872	2871	2862/82	2870/75
sp^3 CH	2920	2890	2890	2900	2890	2900/15
sp^3 CH_2 asym	2920	2926	2926	2927	2916/36	2915/30
sp^3 CH_3 asym	2970	2962	2962	2954/88	2952/72	2959
sp^2 CH_2 sym	2945				2980/3000	2975/80
sp^2 CH olef.	3000	3010/40	3010/40	3015/30	3000/20	3014/35
sp^2 CH_2 asym	3025	3075/95	3075/95	3075	3075/90	3063/79
sp^2 CH arom.	3060	3038	3030	3050	3000/3100	3046/58

[a]Reference 11.
[b]Reference 47.
[c]Reference 46.
[d]Reference 43.
[e]Reference 66.

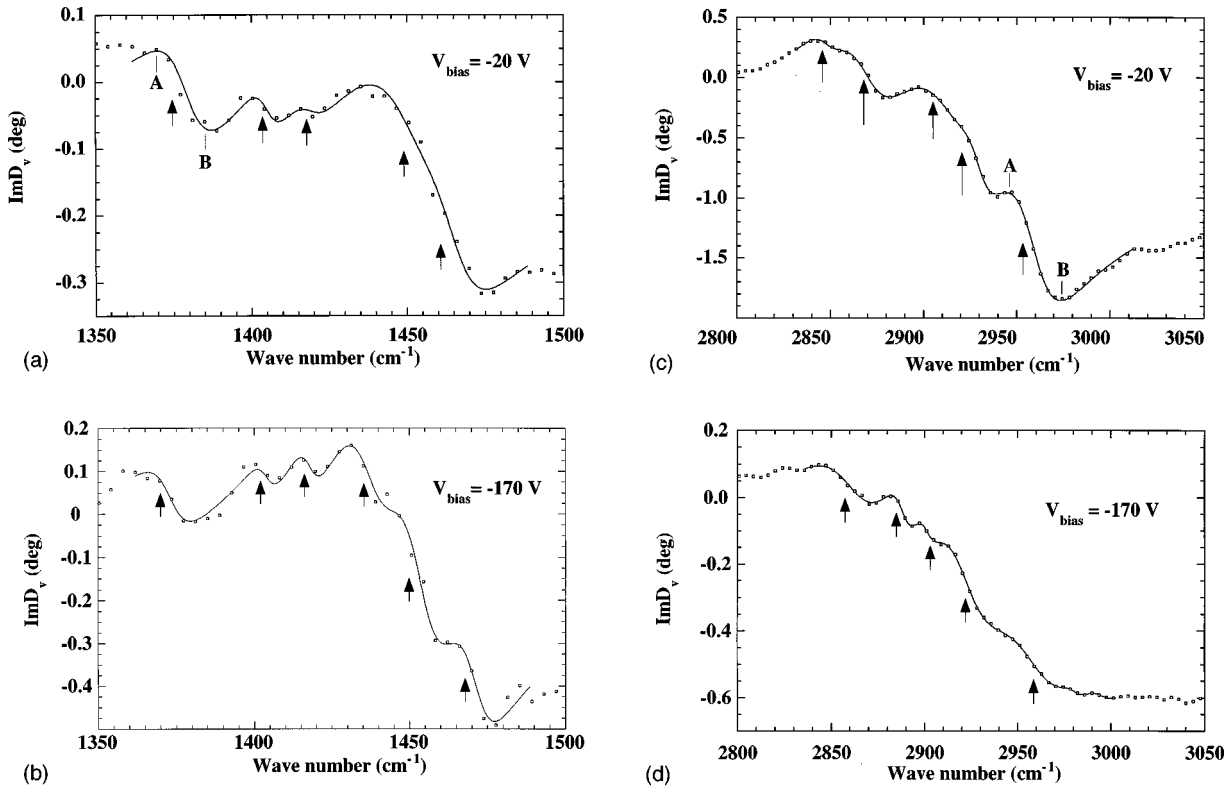

FIG. 4. Examples of decomposition of infrared bending (a) and (b) and stretching (c) and (d) bands for *a*-C:H samples obtained with a self-bias of −20 and −170 V. In (a) and (c) points *A* and *B* allow us to evaluate the bandwidth (see Sec. VII).

in Fig. 4 for two *a*-C:H films deposited with self-biases of −20 (a) and (c) and −170 V (b) and (d). Spectra will be analyzed in detail in the following part but it can directly be observed that C—H bonding evolves with V_{bias} and total hydrogen concentration that varies from 53 at. % (V_{bias}= −20 V) to 40 at. % (V_{bias}= −170 V).

In the bending mode [Figs. 4(a) and 4(b)], the data points are more scattered around the model fit compared with the stretching mode because of a lower signal/noise ratio. Note also that these decompositions have been made using the same set of frequencies (within ± 4 cm^{-1}) and widths (within 15%) for all thicknesses, which gives strong constraints on the decomposition parameters and limits the fit quality.

After fitting procedures, the coefficient of each Lorentzian shape corresponding to a particular vibration and representing the absorption intensity [see Eqs. (5) and (6)] is plotted as a function of deposition time. Figures 5(a) and 5(b), which include some examples of absorption intensities as a function of deposition time for different vibrational configurations, show a linear evolution. Carefully looking at Fig. 5(a), one can observe that a least-square linear fit to the data does not exactly yield a zero intercept. This discrepancy, which remains faint, may be interpreted in terms of interface formation between film and substrate.

Spectra analysis has shown that for all films and all considered vibrations, a linear evolution of the absorption intensity versus time deposition is observed, at least above 200 Å. In the present work, only the linear region, corresponding to thicknesses varying from 300 to 3000 Å, will be taken into account [see Fig. 5(b)]. Surface and interface phenomena are described in Refs. 21 and 40, showing that, in the same conditions of ion bombardment, the interface and top layer are at most 50 Å thick.

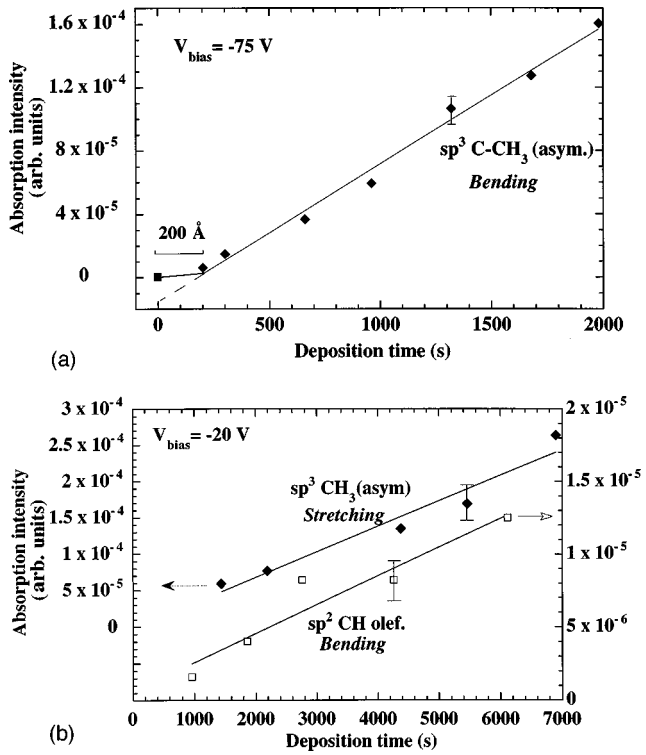

FIG. 5. Absorption intensity as a function of deposition time for different vibrations and deposition conditions: sp^3 C—CH_3 in the bending mode (a) and sp^3 CH_3 (asym) in the stretching mode with olefinic sp^2 CH in the bending mode (b). The lines are linear fits corresponding to the homogeneous growth regime.

TABLE IV. Frequency evolution of sp^3 CH_n bending band in presence of π bond in β.

Group	Symmetry	Wexler[a]	This work
—C—CH_3	sym	1379	1380
	asym	1458/67	1465
═C—CH_3	sym	1370	1360/70
	asym	1440	1437
—C—CH_2–		1467	1450
═C—CH_2		1467	1450

[a]References 17 and 43.

In the linear region, the slope has the expression

$$p_2 = 4\pi \sin\theta_0 \tan\theta_0 \frac{1}{\varepsilon_\infty^2} f\sigma_0 R_d . \tag{18}$$

Compared with previous procedures,[10,12] this method allows us to distinguish bulk from surface properties and to eliminate features that do not physically correspond to vibrations. From Eq. (6) f can be related to N and to the dynamical charge of the group vibration:

$$f = \frac{Ne^{*2} f_{\text{int}}^2}{1.89\times 10^{16}\sigma_0^2}, \tag{19}$$

where N is a number of oscillators per cm^3 and σ_0 is expressed in cm^{-1}.

V. ORGANIC COMPOUND DATA

A. Band frequencies

In order to analyze IR spectra and to compare our results with those of the literature, Table II presents a frequency list of CH_n vibrations. Some data of Dischler[11] for plasma deposited a-C:H films do not correspond to frequencies mentioned in organic compound IR handbooks. Among the problems found in experimental characterizations, it should be noticed that sp^2 CH aromatic bending band near 1445 cm^{-1} is usually too weak to be observed. Concerning the sp^2 CH_2 olefinic stretching bands, no data evidence clearly the presence of the symmetric mode. The sp^3 CH stretching line position is not precisely defined and reference values can vary from 2890 to 2920 cm^{-1}.

As already mentioned, vibrational properties of sp^3 CH_n groups can be strongly altered by the presence of neighboring π bonds. Table IV shows that π bonds induce a decrease of the sp^3 CH_3 bending frequency in both symmetric and asymmetric modes. In contrast, no other line shift has been reported, neither for sp^3 CH_2 group in the bending mode nor for sp^3 CH_n stretching vibrations.

B. Effective dynamical charges

Thanks to Eqs. (6) and (16), using infrared references of pure hydrocarbons, effective dynamic charges have been calculated for different sp^3 CH_n group vibrations in the bending and stretching modes. The values are reported in Table V. For IR measurements performed in the liquid or gas phase, the Lorentz internal field has been considered. The values of Fox[16] should be taken with care because we had to estimate graphically the individual bandwidths. For Jones[41] data, an identical width of 30 cm^{-1} for all vibrations has been supposed. The dynamical charges that seem to be the more reliable are those from Francis[42] and those from the review of Wexler,[43] since no assumptions have been made on the bandwidth values. In all of these references, no bond decomposition has been achieved: hydrocarbon molecules have always been assumed to behave like a noninteracting mixture of CH_n groups. Table V also presents dynamical charges of crystalline n paraffins measured by Snyder[44] and those of semicrystalline polypropylene (PP), measured by ourselves. The same Lorentz field correction has been taken into account, n being the refractive index of the organic solids. The e^* values for solid hydrocarbons (crystals or PP) are not so far from those of liquid or gaseous ones, which could indicate that the same e^* set can be used in organic compounds,

TABLE V. Effective dynamical charges (in elementary charge unit) of sp^3 CH_n groups. Polypropylene (PP) has been measured by us.

		Reference						
Group	Mode	Francis[a]	Fox[b]	Jones[c]	Luther[d]	Wexler[e]	Snyder[f]	PP
sp^3 CH_3 (asym)	Bending	0.046		0.054	0.038	0.054	0.025	
sp^3 CH_2	Bending	0.036		0.035	0.034	0.041	0.052	
sp^3 CH_3 (sym)	Bending	0.055		0.041	0.059	0.064	0.044	
sp^3 CH_2 (sym)	Stretching	0.084	0.068	0.081		0.090	0.090	0.096
sp^3 CH_3 (sym)	Stretching	0.051	0.074	0.088		0.106	0.062	0.117
sp^3 CH	Stretching	0.092	0.025			0.115		0.042
sp^3 CH_2 (asym)	Stretching	0.145	0.109	0.105		0.153	0.122	0.136
sp^3 CH_3 (asym)	Stretching	0.156	0.121	0.136		0.165	0.138	0.149

[a]Reference 42.
[b]Reference 16.
[c]Reference 41.
[d]Reference 67.
[e]References 17 and 43.
[f]Reference 44.

TABLE VI. Effective dynamical charges (in e unit) of sp^3 CH_n groups bonded to sp^2 carbon.

Group configuration	Mode and symmetry	e^*[a]
$=C—CH_3$	Bending (sym)	0.068
	Bending (asym)	0.087
	Stretching (sym)	0.079
	Stretching (asym)	0.124
$=C—CH_2$	Bending	0.056
	Stretching (sym)	0.065
	Stretching (asym)	0.111

[a]References 17 and 43.

irrespective of the matter state. In Table VI the dependence of e^* with the local environment is shown, compared with Wexler's data in Table V. In the presence of π bonds in the β position (i.e., second neighbor), hyperconjugation,[45] which results from a charge transfer between C=C and CH groups, occurs and leads to an increase of e^*_{ben} and a decrease of e^*_{str}, respectively, in the bending and stretching modes.

In Table VII, e^* values for sp^2 CH_n groups have been calculated in olefinic and aromatic configurations showing that they are of same order of magnitude as for sp^3 CH_n groups. However, Bellamy[46] and Rao[47] have stated that the vibrations of monohydrogenated olefinic groups ($R_1R_2C=CHR_3$) are too weak to be observed. Rao[47] mentions that aromatic CH bending bands (near 1450 cm^{-1}) are rarely observed since they are frequently overlaid by CH_2 deformation.

VI. RESULTS

As already mentioned, for all samples, the evolution of Im D (off band) and of the vibration intensities versus deposition time are linear at least above 200 Å (see Figs. 2 and 5), which indicates that the growth is homogeneous[21] in the considered region and that the analysis characterizes well and truly bulk properties. Before analyzing the evolution of C—H bonding versus V_{bias}, density and IR dielectric function are determined by combining ERD, IR, and UV-visible ellipsometric measurements. In Fig. 6, the increase of the dielectric constant with increasing self-bias voltage shows the role of ion bombardment that is favoring the formation of π bonds[48] and densifying the films. sp^2 content increases with ion energy and the hydrogen content decreases as already mentioned from 53 to 40 at. %. Figure 6 also indicates

TABLE VII. Effective dynamical charges (in e unit) of sp^2 CH_n structural units. ϕ is the symbol used for the phenyl group.

Group configuration	Mode and symmetry	e^*[a]
$—C=CH_2$	CH_2 bending	0.046
	CH_2 stretching (asym)	0.096
$R_1HC=CHR_2$	CH in plane deformation	0.069
cis-$R_1HC=CHR_2$	Stretching	0.152
trans-$R_1HC=CHR_2$	Stretching	0.106
ϕ-CH	Stretching	0.065

[a]References 17 and 43.

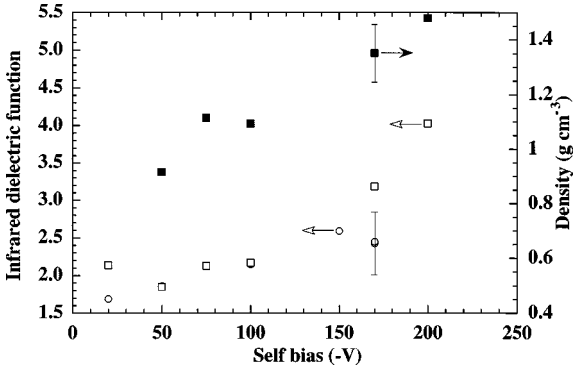

FIG. 6. Infrared dielectric constant (ε_∞) and density (solid squares) of a-C:H films as a function of self-bias (negative values). Two detectors have been used to determine ε_∞ : $Hg_xCd_{1-x}Te$ (open squares) and InSb (open circles). A typical error bar is plotted.

that ε_∞, which corresponds to the film optical response in the IR transparency regions, is strongly related to the atomic density. The linear background in IR ellipsometric spectra could thus be used to evaluate easily a-C:H film density.

To understand more deeply the evolution of a-C:H structure versus V_{bias}, vibrations associated with CH_3, CH_2, and CH units have been studied in detail in both bending and stretching modes. For methyl and methylene groups, the determination of the effective charges will be based on the analysis of intensity ratio between (sym)/(asym) and stretching/bending modes. No local field correction is needed in that case. For CH units, e^* will be studied as a function of self-bias: ERD measurements and Lorentz local field factor will then be used to calculate e^* and oscillator densities.

A. CH_3 group

1. Bending mode

As shown in Fig. 4, the 1350–1500 cm^{-1} region has been decomposed using six vibrations at 1370/80, 1404, 1418, 1437, 1450, and 1465 cm^{-1}. Errors bar amplitudes are ± 4 cm^{-1} on the line positions. Figure 7 indicates that the frequencies are constant within 5 cm^{-1} except for the 1370/80 cm^{-1} mode, which can be unambiguously attributed to symmetric (sym) sp^3 CH_3 bending including both ($=C—CH_3$) and ($—C—CH_3$) units (see Table II). According to Table IV, the slight decrease of the sp^3 CH_3 (sym) is related to the presence of sp^2 carbons bonded to the methyl group. In such

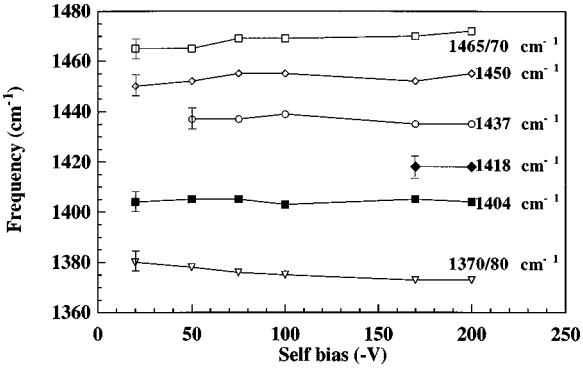

FIG. 7. Line positions of sp^3 CH_n and sp^2 CH_n groups vs self-bias (bending mode).

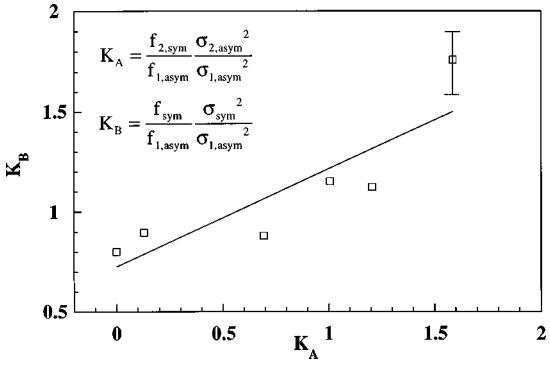

FIG. 8. Bending intensity ratio K_A and K_B as function of each other (hypothesis *B*). The solid line is the model assessing constant effective charges.

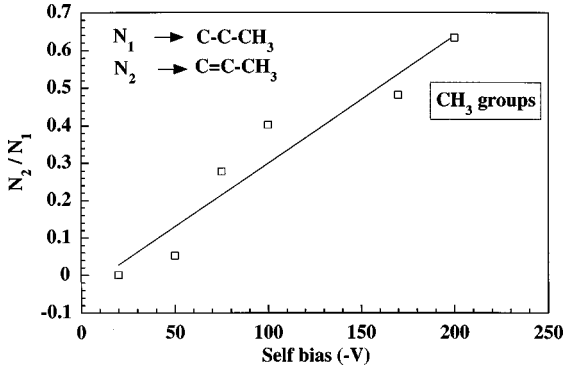

FIG. 9. Evolution of the methyl group local environment. N_1 and N_2 are the numbers of CH_3 groups attached to a sp^3 or sp^2 carbon, respectively. The solid line is a guide for the eye.

a case, Table IV shows that the sp^3 CH_3 (asym) mode frequency should also decrease from 1450/65 to 1440 cm^{-1}. Consequently, the 1437 ± 4 cm^{-1} vibration is attributed to the asymmetric (═C—CH_3) mode. The asymmetric (—C—CH_3) mode is located either at 1450 cm^{-1} (hypothesis *A*) or at 1465 cm^{-1} (hypothesis *B*). Using Eq. (19), a relation between the vibrational intensity of (sym) and (asym) modes can be established:

$$(e^*_{1,\mathrm{sym}})^2 + (e^*_{2,\mathrm{sym}})^2 \frac{(e^*_{1,\mathrm{asym}})^2}{(e^*_{2,\mathrm{asym}})^2} K_A = (e^*_{1,\mathrm{asym}})^2 K_B, \quad (20)$$

where

$$K_A = \frac{f_{2,\mathrm{asym}}}{f_{1,\mathrm{asym}}} \frac{(\sigma_{2,\mathrm{asym}})^2}{(\sigma_{1,\mathrm{asym}})^2}, \quad (21)$$

$$K_B = \frac{f_{\mathrm{sym}}}{f_{1,\mathrm{asym}}} \frac{(\sigma_{\mathrm{sym}})^2}{(\sigma_{1,\mathrm{asym}})^2}. \quad (22)$$

The indices 1 and 2 characterize the (—C—CH_3) and (═C—CH_3) groups, of respective densities N_1 and N_2. At low self-bias, no clear vibration at 1437 cm^{-1} is present, indicating that $N_2 \ll N_1$. We can thus calculate the square of effective charges ratio between (asym) and (sym) (—C—CH_3) modes. Values of 0.43 and 0.80 are found for hypotheses *A* and *B*, compared with an average 0.71 ratio in free molecules, which shows that the 1465-cm^{-1} mode is certainly associated with the (—C—CH_3) group. Moreover, Eq. (20) stipulates that, if effective charges in *a*-C:H are constant, K_A and K_B are related by a linear law. Figure 8 shows that, within the error margin, this assumption is fair. Through slope analysis, the ratio $e^*_{2,\mathrm{sym}}/e^*_{2,\mathrm{asym}}$ can be determined. Taking as reference $e^*_{1,\mathrm{sym}}$ and $e^*_{1,\mathrm{asym}}$ values given by Wexler,[43] sp^3 CH_3 bending effective charges are calculated and reported in Table VIII. In Fig. 9, the fraction of N_1 and N_2 is plotted versus V_{bias}, indicating that the local environment of methyl groups evolves from sp^3 to a mixture of sp^2/sp^3-configurated carbon atoms.

TABLE VIII. Effective charges of CH_3 in bending and stretching modes. In our calculations, the underlined values are taken from Wexler.[a]

Group	Mode	Wexler[a]	This work
—C—CH_3 (sym)	Bending	0.054	<u>0.054</u>
—C—CH_3 (asym)	Bending	0.064	<u>0.064</u>
═C—CH_3 (sym)	Bending	0.068	0.060
═C—CH_3 (asym)	Bending	0.087	0.090
—C—CH_3 (sym)	Stretching	0.106	0.117
—C—CH_3 (asym)	Stretching	0.165	<u>0.165</u>
═C—CH_3 (sym)	Stretching	0.079	0.085
═C—CH_3 (asym)	Stretching	0.124	0.120

[a]Reference 43.

2. Stretching mode

Figure 4 shows the result of band decomposition in the 2840–2980 cm^{-1} stretching region. This region can be decomposed using five vibrations at 2845/60, 2870/75, 2900/15, 2915/30, and 2959 cm^{-1}. It will be demonstrated in the following sections that this decomposition cannot be performed with less than five bands. The evolution of band frequency with V_{bias} is plotted in Fig. 10. According to Table III, the 2870/75 and 2959 cm^{-1} vibrations are attributed to methyl groups (sp^3 CH_3) whereas the 2845/60 and 2915/30 cm^{-1} inflections characterize methylene groups (sp^3 CH_2). Vibrations located at 2900/15 cm^{-1} are attributed to sp^3 CH groups. Methyl group line positions in (sym) and (asym) modes stay constant whereas frequency shift can be observed for methylene and CH units. It is evident from Table VI that different effective charges should be assumed for

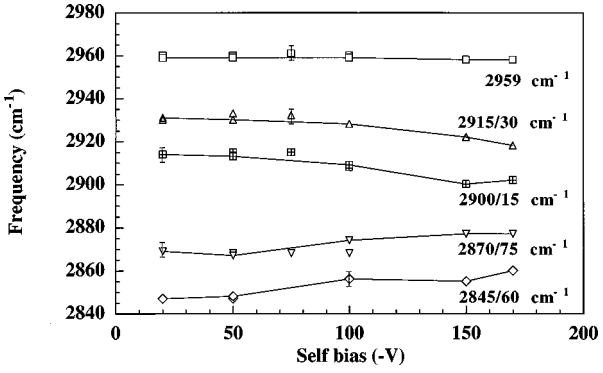

FIG. 10. Line positions of sp^3 CH_n group vs self-bias (stretching mode).

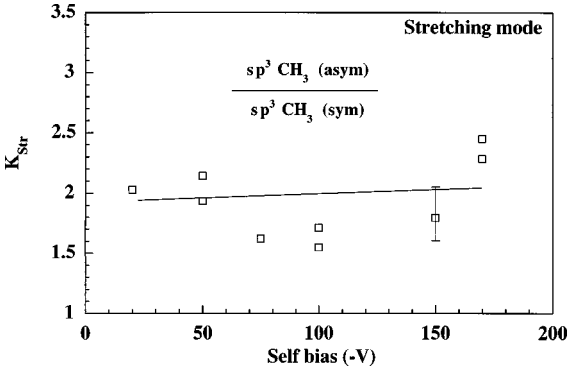

FIG. 11. Asymmetric to symmetric stretching intensity ratio (K_{Str}) vs self-bias: the open squares are experimental points; the solid line is the fit assessing constant effective charges.

CH_3:$e^*_{1,2870}$, $e^*_{2,2870}$, $e^*_{1,2959}$, and $e^*_{2,2959}$, the first and second index designating the type of environment (see previous section) and the vibrational frequency, respectively. Using Eq. (19), it can be shown that

$$K_{\mathrm{Str}}=\frac{(e^*_{1,2959})^2+\frac{N_2}{N_1}(e^*_{2,2959})^2}{(e^*_{1,2870})^2+\frac{N_2}{N_1}(e^*_{2,2870})^2}, \tag{23}$$

where

$$K_{\mathrm{Str}}=\frac{f_{2959}}{f_{2870}}\frac{(\sigma_{2959})^2}{(\sigma_{2870})^2}. \tag{24}$$

The N_2/N_1 ratio has been previously determined for bending modes. Taking as a reference the average value of $e^*_{1,2959}$ given by Wexler and the quantitative effect of hyperconjugation, the other effective charges can be calculated by fitting experimental results with Eq. (23). These are reported in Table VIII and are in good agreement with effective charges of organic molecules. Figure 11 compares experimental data with our model based on constant effective charges. According to these results, owing to the values of e^*_2 compared with e^*_1, a constant ratio for (sym) and (asym) sp^3 CH_3 vibrations within a 25% error can be supposed in the decomposition of IR spectra. This result remains valid at all values of N_2/N_1. This latter statement has often been supposed for the decomposition of all modes of IR spectra but no clear confirmation had been given up to now.

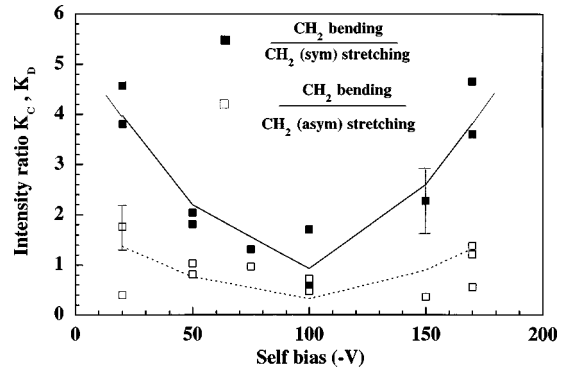

FIG. 12. Intensity ratios of sp^3 CH_2 groups in the bending mode, to the symmetric and asymmetric stretching modes.

TABLE IX. Effective charges of sp^3 methylene groups used to fit experimental results.

Group	Mode	e^*
—C—CH_2–	Bending	0.041
═C—CH_2	Bending	0.26
—C—CH_2– (sym)	Stretching	0.090
—C—CH_2– (asym)	Stretching	0.153
═C—CH_2 (sym)	Stretching	0.065
═C—CH_2 (asym)	Stretching	0.111

B. sp^3 CH_2 group

From our fitting procedures, the 1450, 2845/60, and 2915/30-cm^{-1} bands have been attributed to sp^3 CH_2 bending, symmetric and asymmetric stretching vibrations, in agreement with values of Tables II and III. As in the case of methyl groups, one has to consider different types of local environments. However, CH_2 local environment description is more complicated since methylene groups can be attached to 0, 1, or 2 π bonds. As a consequence, two types of surroundings will be considered: methylene units bonded either to two sp^3 carbon (—C—CH_2—C) or to, at least, one sp^2 carbon (═C—CH_2). N'_1 and N'_2 will designate the respective densities of these groups. Ratios between different sp^3 CH_2 vibrational modes can again be defined:

$$K_C=\frac{f_{1450}}{f_{2920}}\frac{(\sigma_{1450})^2}{(\sigma_{2920})^2}, \tag{25}$$

$$K_D=\frac{f_{1450}}{f_{2820}}\frac{(\sigma_{1450})^2}{(\sigma_{2850})^2}. \tag{26}$$

Figure 12 shows that, even if error bars are taken into account, K_C and K_D are not monotonous versus self-bias, in contrast to K_A, K_B, and K_{Str}. This experimental result can be explained by (i) a strong evolution of CH_2 effective charges in a-C:H, and (ii) a N'_2/N'_1 ratio, which is not a monotonous function of self-bias. As far as hypothesis (i) is concerned, we have proved in a previous section that effective charges of organic compounds are well adapted to de-

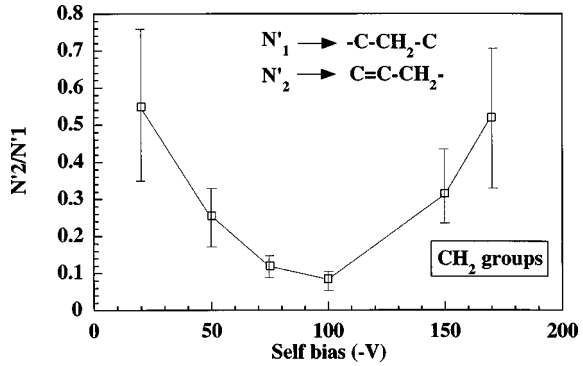

FIG. 13. Evolution of the sp^3 CH_2 local environment. N'_1 and N'_2 are the numbers of CH_2 groups attached to a sp^3 or sp^2 carbon, respectively.

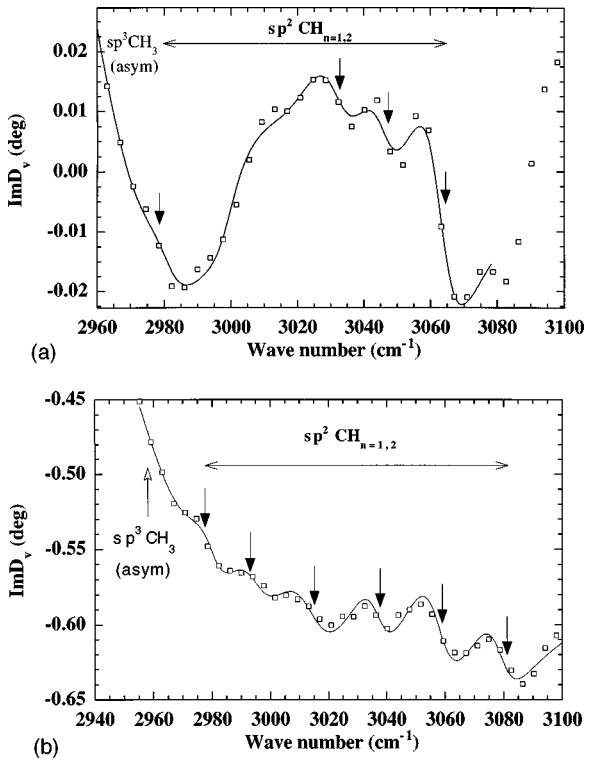

FIG. 14. Vibrational spectra of the 3000 cm^{-1} region for films deposited at -150 (a) and -170 V (b) self-bias. Open squares correspond to experimental results. The solid lines are the fits resulting from decomposition.

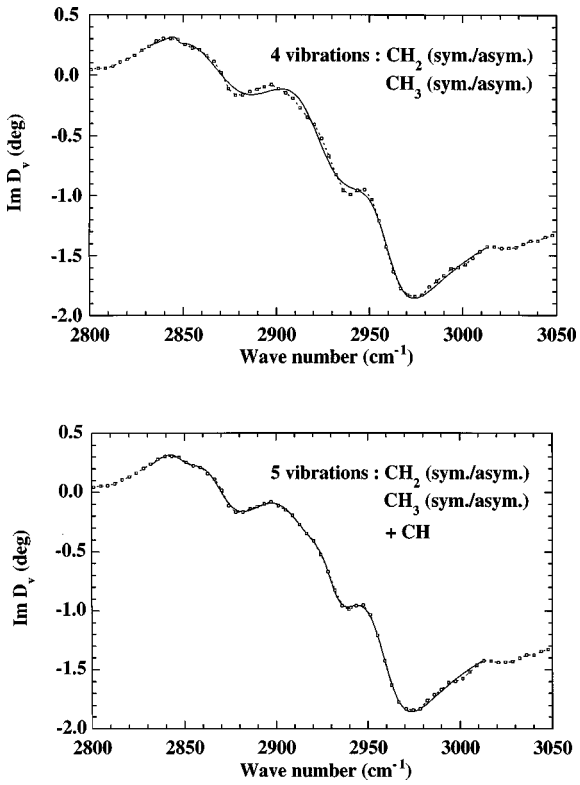

FIG. 15. Decomposition of the stretching region using either four or five Lorentz oscillators.

scribe the vibrational intensities of methyl groups. We will thus use constant e^* values as obtained from organic chemistry and consider hypothesis (ii). In order to describe the nonmonotonous N_2'/N_1' ratio, a second-order polynomial function of V_{bias} has been chosen. Experimental K_C and K_D curves plotted in Fig. 12 can be fairly modeled by using effective charges reported in Table IX and three parameters characterizing the polynomial N_2'/N_1' evolution. The relative group densities (N_1' and N_2') are plotted in Fig. 13. Note that error bars are quite important but the N_2'/N_1' ratio cannot be considered as a constant: the evolution is clearly nonmonotonous. Contrary to the methyl case, N_2' does not represent the density of one precise group but takes into account all the types of environment that contain at least one π bond, which could explain the rather complex evolution of N_2'/N_1'. The observed minimum at $V_{\text{bias}} = -100$ V, which may suggest a structural transition, will be interpreted below.

C. sp^2 CH_n group

1. Bending mode

Figure 4 clearly evidences vibrations located at 1404 and 1418 cm^{-1}, which do not correspond to sp^3 CH_n groups (see Table II). In comparison with organic molecules, these modes are attributed to sp^2 CH in olefinic configuration and to sp^2 CH_2, respectively. The latter is only detected for samples deposited at high ion energy whereas the former can be observed at all values of self-bias (see Fig. 7). Our observations do not correspond to Dischler's attribution (see Table III) and prove that our films always contain a certain amount of π bonds: a purely hydrogenated sp^3 network cannot be obtained, even at very low ion energy.

2. Stretching mode

As we discussed in Sec. I, the contribution of the (asym) methyl group to IR absorption is high in the stretching region. Thus the IR signal of sp^2 CH_n vibrations, which is expected in the 2950/3100-cm^{-1} range, cannot be easily detected. Only for samples having a relatively low methyl IR signal, band analysis can be performed in this region. Figure 14 shows IR spectra and their decomposition which evidence many vibrational modes. The fits are not as good as those presented in Fig. 4 but still allow us to localize vibrations and to determine line positions. Band attribution is presented in Table III, in good agreement with line positions of organic molecules. The 3014 and 3035-cm^{-1} bands certainly characterize sp^2 CH olefinic bonds in, respectively, cis and trans (—CH═CH-) configurations. As in the bending mode, the sp^2 $CH_{n=1,2}$ bandwidths are between 15 and 25 cm^{-1}, and remain low as compared to the 25–50 cm^{-1} values found for methyl or methylene groups. No evaluation of effective charges has been performed, in view of the very small IR signal amplitude.

D. sp^3 CH group

The sp^3 CH stretching vibration is known to be difficult to detect: its presence is often obscured by the stronger methylene and methyl group absorption. This band, which can be directly observed for films deposited using a high V_{bias} value, has also been evidenced through fitting procedures. Figure 15 presents two types of decompositions using either

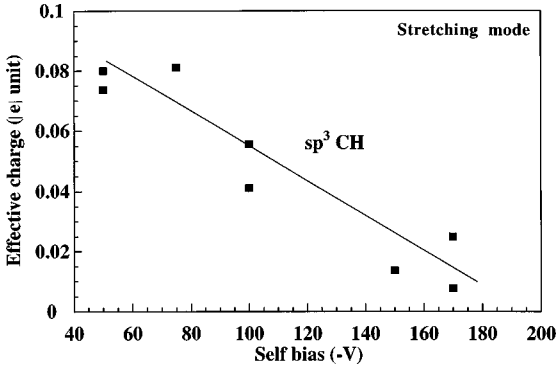

FIG. 16. Effective charge of sp^3 CH stretching mode as a function of self-bias. The line is a linear fit.

four or five different bands, i.e., sp^3 CH_3 and sp^3 CH_2 in (asym) and (sym) modes combined or not with a vibrational mode located around 2900 cm^{-1}. The different bandwidths have been limited to 50 cm^{-1} so that the fit could converge properly towards meaningful parameters. Figure 15 clearly evidences the sp^3 CH band located between sp^3 CH_3 (sym) and sp^3 CH_2 (asym) vibrations.

The analysis method that has been performed to determine e^* for CH_2 and CH_3 units cannot be used for the CH group since its vibrational modes are not separated in (sym) and (asym) normal modes. Moreover, no clear CH bending vibrations have been observed. At last, as shown in Table V, the sp^3 CH effective charge values (e^*_{2900}) in the stretching mode calculated from different references show a high dispersion, in contrast to other CH_n groups. Even for saturated hydrocarbons, IR spectra can hardly be fitted using a constant effective charge.[17]

In order to calculate e^*_{2900}, the following assumptions are made: (i) almost all hydrogen atoms measured by ERD are bonded to carbon and are thus IR active; (ii) effective charges of sp^2 CH_n vibrations are of the same order of magnitude as those presented in Table VII.

The first assumption is based on results reported by Honeybone and co-workers[10,49] showing that only small quantities of molecular hydrogen are trapped inside a-C:H films. Using hypothesis (ii) and comparing absorption intensities of sp^2 $CH_{n=1,2}$ and sp^3 $CH_{n=2,3}$ bending groups, it can be concluded that hydrogen is essentially bonded to sp^3 carbon

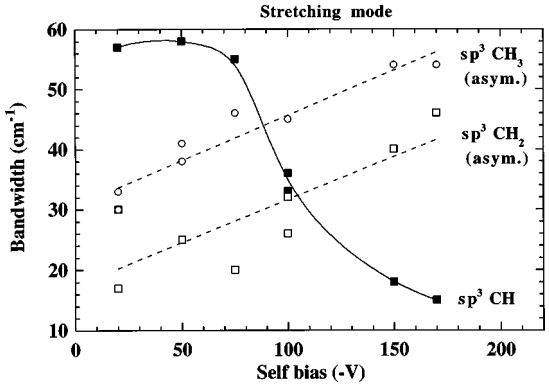

FIG. 17. Bandwidths of sp^3 CH (solid squares), CH_2 (open squares), and CH_3 (open circles) groups in the stretching mode vs self-bias. Dashed and solid lines are guides for the eye.

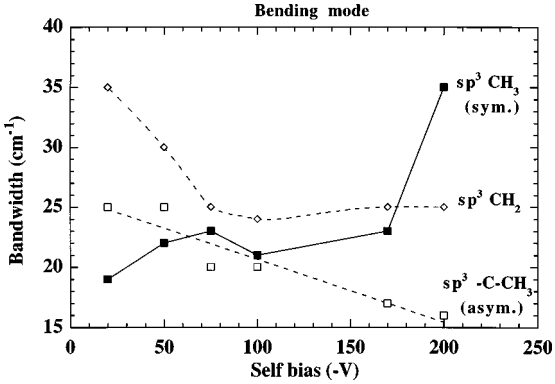

FIG. 18. Bandwidths of sp^3 CH_3 (sym) (solid squares), —C—CH_3 (asym) (open squares), and sp^3 CH_2 (open diamonds) groups in the bending mode vs self-bias. Dashed and solid lines are guides for the eye.

atoms, consistent with previous results.[7,10] The total IR active hydrogen amount can thus be calculated without taking into account the sp^2 CH_n groups.[50] The total number of CH_2 and CH_3 units (N_m) is calculated using results of previous parts and the Lorentz field correction. Thanks to hypotheses (i) and (ii), the number of sp^3 CH bonds can be deduced using ERD measurements and the N_m values. e^*_{2900} can then be evaluated as a function of self-bias. f_{int} is again assumed to correspond to the expression given by Lorentz. In Fig. 16, the evolution of sp^3 CH effective charge versus V_{bias} is shown revealing a strong decrease of e^*_{2900} from 0.08 to 0.02.

E. Bandwidths

Bandwidths are deduced from decomposition procedures. For isolated vibrations like sp^3 CH_3 (sym) in the bending mode or vibrations that are not followed by another one, like sp^3 CH_3 (asym) in the stretching mode, the width can be evaluated by the eye by looking at the local extrema of Im D_v [see points A and B of Figs. 4(a) and 4(c)]. The distance (in cm^{-1}) between A and B is a first evaluation of Γ. As a matter of fact, bandwidths of sp^3 CH_3 (sym, bending mode) and sp^3 CH_3 (asym, stretching mode) vibrations can be evaluated by the eye. For $V_{\text{bias}}=-20$ V, respective values of 16 and 28 cm^{-1} are found whereas the decomposition leads to values of 19 and 33 cm^{-1}, respectively. When inflections are surrounded by others, like sp^3 CH or sp^3 CH_2, the only way of determining bandwidths is to perform decomposition. In order to get reasonable values, the maximum value of Γ is set to 60 cm^{-1} for all vibrations.

Bandwidths of principal vibrations are presented in Figs. 17 and 18 versus V_{bias}. In the stretching mode, methyl and methylene (asym) peak widths are nearly the same and become larger when ion energy increases: for these vibrations, Γ reaches 50 cm^{-1} for $V_{\text{bias}}=-170$ V. In contrast, sp^3 CH bandwidth decreases versus self-bias, from 55 to 15 cm^{-1}. In the bending mode, the (asym) vibrations become sharper with increasing ion energy whereas broadening is seen for the 1370/80-cm^{-1} mode. These results show that bandwidth evolution is not straightforward and can depend on the vibrational mode as on the CH_n group. In Sec. VII, it will be shown that bandwidth and effective charge are closely related.

VII. DISCUSSION

The analysis method we have developed has allowed us to determine in detail the vibrational properties of *a*-C:H films; that is, frequency, bandwidth, and effective charge for each sp^3 CH_n group. In the present study, *in situ* ellipsometry has been used to measure absorption intensities as a function of deposition time. In the homogeneous growth regime, which is characterized by a linear evolution of Im *D* and absorption intensities versus deposition time, band decompositions on more than five spectra have been performed, as compared to one in standard IR analysis. The calculation of *f* is performed through slope analysis [see Eq. (18)], which provides good precision. Another advantage of using ellipsometry concerns the IR background. Using classical IR absorption techniques, *a*-C:H film thickness should be high enough to get a reasonable signal/noise ratio. Spectra background is affected by fringes and becomes a complex function of thickness and refractive index.[19] In our case, as measurements are performed on thin films, the background shape is linear, which makes its subtraction easier and vibrational studies more reliable, especially for near absorption edge bands.

Thanks to our analysis method, C—H bonding properties have been determined in terms of frequency, bandwidth, and effective charge. H distribution, sp^2 content, and density evolve with V_{bias} as shown in Fig. 6. First neighbors of methyl groups evolve from purely sp^3 to a mixture of sp^3/sp^2 configurated carbons. For methylene groups, the change of local environment is more complex as indicated in Fig. 13. The calculation of CH stretching effective charge reveals that the absorption strength of a monohydrogenated carbon can strongly evolve with *a*-C:H microstructure. In order to explain C—H bonding properties, a local description of vibrational modes will be used. At first, the discussion will deal with local field effects. The Lorentz correction that has always been assumed will be discussed. Second, line broadening and shift observed in Sec. VI will be explained. A particular section will be devoted to effective charge values calculated for sp^3 CH_n bonds. From all this analysis, consideration of *a*-C:H microstructure will, finally, be presented.

A. Local field

In the calculation of effective charge ratios for methyl and methylene units, no assumption has been made on the expression of the local field correction. However, in the determination of e^*_{2900}, a Lorentz-type f_{int} factor has been considered to evaluate the total C—H oscillator density. One should question if such a correction is accurate. The Lorentz local field has been proved to be a good approximation for gas and liquid-phase hydrocarbons. In solid phase, the internal field depends not only on the dielectric polarizability but also on the dipole concentration and on the atom density. Hence, in the case of *a*-Si:H where H/Si is low (approximately 0.05–0.1), as H is assumed to be randomly distributed throughout the *a*-Si phase, each Si—H bound can be locally represented by a dipole oscillating in a cavity, surrounded by a nonhydrogenated silicon matrix. The contrast between the dielectric function void and *a*-Si ($\varepsilon_{a\text{-Si}}$) is high and can lead to strong evolution of f_{int} if the cavity is deformed.[33,34] Moreover, as $\varepsilon_{a\text{-Si}}$ is high, the Lorentz and Onsager internal fields take values that can differ by an order of magnitude.

In the case of polymerlike carbon, film density and dielectric function values are relatively low (from 0.8 to 1.5 g/cm^3 and from 1.5 to 4.5, respectively). The ratio H/C evolves from 1.1 to 0.7. The particular effects described for *a*-Si:H are thus no more valid. Moreover, owing to the high H concentration, the different CH groups cannot be considered as isolated dipoles in a nonhydrogenated carbon matrix. As the C—H dipoles make up in great part the dielectric medium, the Lorentz local field correction seems to be better adapted for polymerlike carbon, as done in this paper.

B. Bandwidth and line frequency

The evolution of bandwidths versus self-bias shown in Figs. 17 and 18 indicates that line broadening depends on the vibrational mode and on the type of CH_n group. Many authors[51,7,52] have tentatively explained the increase of CH stretching bandwidth by assuming that strain effects become stronger as ion energy increases. Couderc[7] has shown that, in *a*-C:H films, stress is compressive and increases as H is lost and density increases. If bandwidth is assumed to be directly related to stress, crosslinking,[7] or density, broadening is then expected to be higher for sp^3 CH units that are located in less hydrogenated regions than for CH_2 or CH_3 groups. This assessment is in contradiction with experimental results shown in Fig. 17. Moreover, this direct description predicts that mechanical stress, which induces length variation and angle distortion, should similarly broaden both bending and stretching CH_n bands. Figures 17 and 18 clearly show that this simple way of interpreting bandwidth is not correct.

Let us recall that, in IR spectroscopy, broadening can be either homogeneous or inhomogeneous. In the former case, width is a consequence of lifetime of excited states and vibrational coupling leading to dephasing phenomena.[53] Such effects are negligible when amorphous film bulk is studied. As vibrational lines result from resonant CH bond oscillations, each one having a particular geometrical and electronical environment, broadening is inhomogeneous and may come from[54] (i) local strain, (ii) local electric field, (iii) interaction with phonons or CH mutual interactions. As mass difference between C and H atoms is strong, as the vibration takes place in a solid where the number of bonded atoms is largely higher than for a free molecule, each CH_n group is assumed to oscillate in a local mode. Interactions with phonons, which should lead to particular vibrational bands, can then be negligible. Quadratic CH mutual interactions are taken into account in the f_{int} factor, as has been explained in previous sections. In the context of a first-order perturbation theory, the line transition energy σ for each vibrational site *i* can be expressed as a function of local strain and electric field:

$$\sigma(i)=\sigma_0+\Sigma_{\text{strain}}(i)e(i)+\Sigma_{\text{electric}}(i)f_{\text{int}}(i), \qquad (27)$$

where σ_0 is the resonant frequency for a free molecule, $e(i)$ and $f_{\text{int}}(i)$ the local stress and field factor; Σ_{strain} and Σ_{electric} are coupling terms that characterize the linear response of the oscillating dipole to the perturbation. These terms are strongly dependent on the effective charge values.

Let us consider first the case of dipoles distributed in a regular lattice structure. It can be shown, through Eq. (27), that frequency of the normal stretching mode shifts owing to dielectric screening. This shift has the approximated expression[55]

$$\Delta\sigma = \frac{\sigma_0}{2}\frac{e^{*2}}{\mu\omega_0} W, \tag{28}$$

where W is proportional to the cube of an interaction length representing the contribution of other dipoles to the local field. Equation (28) describes how effective charge variations can influence inhomogeneous broadening. Taking a typical value[56] of 0.5 Å^3 for W, the frequency shift of the sp^3 CH stretching band due to effective charge evolution (see Fig. 10) can be calculated. A downshift value of 15 cm^{-1} is found, very similar to the experimental shift. Moreover, Eq. (28) predicts that broadening (i.e., shift from σ_0) decreases when e^* is lowered, consistent with bandwidths plotted in Fig. 17. For CH_2 and CH_3 group stretching vibrations, the effective charges do not change much to induce significant variations of linewidth by screening effects.

Local angle distortions and length variations, resulting from local stress, will affect effective charges values [see Eqs. (14) and (15)]. The coupling term Σ_{strain} increases as the oscillating group is more sensitive to environment, i.e., as e^* is higher. Therefore, the strain influence on the sp^3 CH stretching group is expected to be far lower than for CH_3 and CH_2 units: the effective charge of the sp^3 CH group is indeed between three and eight times lower than that of sp^3 $CH_{n=2,3}$ units. Concerning methylene groups, by comparing width evolution of stretching and bending regions and using Eqs. (14) and (15), we can conclude that bond length variation does not affect much line broadening (a small decrease for the 1450-cm^{-1} line). Broadening of stretching bands may then come from changes of charge flows. This statement is justified by the fact that $(\partial q_H^0/\partial r_H) r_H^0$ is nearly one order of magnitude higher than q_H^0 in C—H compounds,[38] which means that the charge on hydrogen atoms is very deformable. The solid line plotted in Fig. 18 does not contradict this assertion since the 1370/80-cm^{-1} band is the superposition of two different lines, one due to —C—CH_3 and the other to ═C—CH_3 units.

Figures 4 and 14 show that the bandwidth of sp^2 $CH_{n=1,2}$ groups is low, compared to methyl (sp^3 CH_3) and methylene (sp^3 CH_2) groups, and does not evolve much with ion energy. If sp^2 CH_n effective charges are assumed to be similar in a-C:H films or organic molecules (see Table VII), this very small bandwidth may indicate that hydrogenated sp^2 regions are weakly strained or disordered. This interpretation is consistent with the model developed by Angus,[57] which shows that strain energy is released when π bonds are formed. As the average degree of freedom per atom is higher for sp^2 than for sp^3 carbon, stress is then expected to be stronger in sp^3-rich domains.

This model for broadening effects in a-C:H can also be applied to tetrahedral hydrogenated amorphous carbon (ta-C:H). IR spectra of such a material reveal well-resolved stretching bands[12] whereas ta-C:H is known to be constrained.[58] The above description has shown that a low value of the effective charge can account for such an observation. Vibrational damping is thus only indirectly related to internal stress since it strongly depends on the effective charge.

To sum up, line broadening is both related to the e^* value and to the vibrational mode. Due to the high H charge deformability, sp^3 CH_2 and sp^3 CH_3 bandwidths are very sensitive to strain or disorder.

C. Effective charges

Effective charges evolution determined for sp^3 CH_3 and CH_2 groups can be fairly well interpreted by the hyperconjugation model. As self-bias increases, the nearest neighborhood of methyl groups becomes richer in π bonds. From Fig. 9, the local methyl environment of films deposited with a high ion energy can be modeled as a mixture of —C—CH_3 and ═C—CH_3 units in ratio 3:2. Using the values given in Table I, the average C—H distance in CH_3 units should thus decrease from 1.54 to 1.52 Å (Ref. 38) and the charge localized on hydrogen should increase from 0.045 to 0.052e. The evolution of the effective charges reported in Tables VIII and IX is consistent with the predictions deduced from Eqs. (14) and (15) that is an increase for the bending mode and a decrease for the stretching mode in presence of π bonds in β. The same conclusions can be drawn for methylene groups: *ab initio* calculations performed on simple organic molecules using the Spartan software have also shown that C—H bond length diminishes and the Mulliken charge[39] on hydrogen tends to increase when CH_2 is bonded to π bonds. The values determined for —C—CH_2 and ═C—CH_2 units (see Table VI) can also be interpreted in terms of hyperconjugation. The high value of $e^*_{2,\text{asym}}$ may indicate that a significant fraction of the different kinds of methylene groups are connected to two sp^2 carbons (═C—CH_2—C═).

In contrast, *ab initio* simulations do not reveal any clear change of single C—H bond length in the presence of π bonds in β. The effective charge decrease shown in Fig. 16 cannot be interpreted as a consequence of hyperconjugation. According to Eq. (14), it could be the result of (i) an increase of q_H^0 charge and (ii) a decrease of r_H^0 or $|\partial q_H/\partial r_H|$. Phenomena described in assumptions (i) and (ii) occur when carbon bonded to single H is included in a three-dimensional structure. For example, in some caged hydrocarbons like triamantane,[59] r_H^0 is reduced from 1.11 to 1.09 Å. C—C and C—H bonds may also be part of a distorted network where the C hybridization state is no more purely sp^3 but a combination of sp^2 and sp^3. In such a case, charge flow values can be strongly modified due to the high electronic deformability of the atomic charge.

D. Microstructure

IR results which are reported in the present work represent a contribution to a structural model of a-C:H since they derive new insights in the description of the hydrogenated network. At first, we have shown that, as V_{bias} increases, the nearest environment of methyl groups becomes enriched with π bonds (see Fig. 9): it evolves with ion energy from sp^3 to a mixture of sp^2-sp^3 configurated carbons. As far as methylene group is concerned, the evolution of the effective charges has also proved that a quite important CH_2 fraction

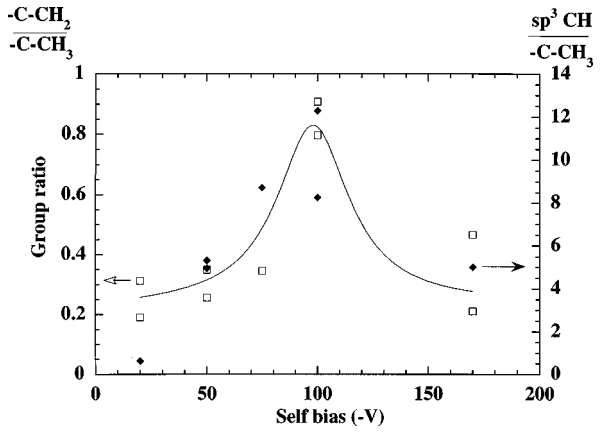

FIG. 19. Group concentration ratios: sp^3 CH vs —C—CH_3 (solid diamonds) and —C—CH_2 vs —C—CH_3 groups (open squares) as a function of self-bias. The line is a guide for the eye.

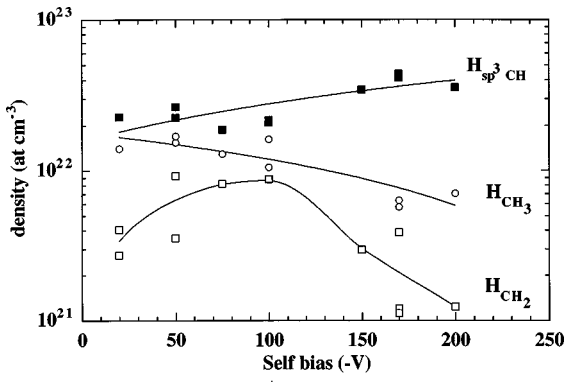

FIG. 20. Density of H atoms bonded to sp^3 carbon involved in CH (solid squares), CH_2 (open squares), and CH_3 (open circles) configurations.

is bonded to sp^2-configured atoms. Figure 13 indicates that the evolution of CH_2 local environment is more complex than CH_3 behavior because methylene can be attached to several sp^2 carbons (=C—CH_2—C=). The minimum observed at $V_{\text{bias}}=-100$ V, which corresponds to densities around 1.2 g/cm^3 (see Fig. 6), indicates a change of the CH_2 neighbor electronic configuration. In contrast to the CH_3 group, which is an ending unit, methylene can be part of a carbon chain. When V_{bias} increases, the change of H distribution can lead to a reorganization of the carbon network. As an illustration, let us recall the reversible transposition reaction (1,3 sigmatropic transposition):

$$\text{—C=C—CH}_2\leftrightarrow\text{—CH—C=CH.} \tag{29}$$

During the film formation,[60] this reaction can explain in part how the number of methylene groups attached to sp^2 carbon (N_2') can easily evolve. The transition at $V_{\text{bias}}=-100$ V also corresponds to the higher fraction of single CH groups compared with CH_3 units bonded to sp^3 as shown in Fig. 19. For this value of V_{bias}, the ratio —C—CH_2/—C—CH_3 corresponds to a maximum too. Figure 19 indicates that the configuration of the saturated polymeric phase does not evolve simply from chains to a crosslinked network. Other authors[12,61,62] have already reported such an evolution interpreted as a transition from polymerlike carbon (PLC) to diamondlike carbon (DLC) films. A extended analysis of the network structure evolution, combining x-ray diffraction and IR ellipsometry,[50] will be reported in another paper.

In Sec. VI C, sp^2 CH (olefinic) and CH_2 bands have been evidenced thanks to our analysis method. The presence of such groups clearly shows that the hydrogenated sp^2 phase does not consist of aromatic clusters that would be hydrogenated at their boundaries. Assuming absorption strengths similar to those of organic compounds, hydrogenated olefinic sp^2 carbon content can be evaluated through bending bands and are found to increase with self-bias from about 5×10^{20} to 3×10^{21} at/cm^3. This result is consistent with the general π bond increase deduced from Fig. 6 and with the evolution of methyl surroundings described above. The increase of the sp^2 fraction with V_{bias} is also correlated with the decrease of the optical gap measured by UV-visible ellipsometric measurements[63] and consistent with most observations.[12,7,10,52] It should be noticed that hydrogen is not equally distributed among the sp^2 and sp^3 phase: in our case, 87–100 % of hydrogen atoms are bonded to sp^3-hybridized atoms.

In order to explain the evolution of the methyl and methylene environment, the two-phase microstructural model consisting of sp^2 clusters embedded in a hydrogenated sp^3-hybridized atom matrix[64,65] has to be modified. π and σ bonds may form a more complicated network, which can be a multiphase heterogeneous structure of saturated/unsaturated polymer and diamondlike regions. In Fig. 20, C—H oscillator densities are calculated for hydrogen atoms involved in simple CH, methyl, and methylene groups. We can observe how hydrogen is distributed inside the polymeric phase. As V_{bias} increases, the number of simple CH groups increases whereas the concentration of H atoms in CH_3 configuration decreases. Figure 20 thus reveals a high fraction of CH groups and a low concentration of methylene units. The model developed by Newport and Walters,[10] consisting of short CH_2 chains and CH groups distributed in a sp^2-sp^3 carbon network with olefinic carbons, is not suitable in our case owing to the relative number of CH, CH_2, and CH_3 units. Figure 20 shows that crosslinking should be important but, comparing CH and CH_3, the end groups are in low concentration. This observation indicates that such a polymeric phase should have a low size: a-C:H microstructure can rather be a mixing, at the atomic scale, of the sp^3/sp^2 network, without distinct phases.

VIII. SUMMARY AND CONCLUSION

A complete C—H bonding study in plasma deposited polymeric a-C:H films has been performed. Using *in situ* IR ellipsometry, an original analysis method has been developed in order to check vibrational bulk properties. IR spectra have been analyzed both inside and outside C—H bands. The simultaneous increase of the IR refractive index and film density reflect the microstructural evolution of a-C:H films. The evolution of IR spectra versus thickness in the homogeneous growth regime has allowed us to determine with accuracy vibration frequencies and widths. Bending and stretching CH regions have indeed been decomposed into separate bands using the same set of bandwidths and line positions for different thicknesses. Calculations of effective charges have

been performed for sp^3 $CH_{n=1,2,3}$ groups: for methylene ($n=2$) and methyl groups ($n=3$), transition dipole moments are constant and similar to those of organic compounds. For the sp^3 CH group, the effective charge has been found to strongly decrease as a function of self-bias during plasma deposition. Line broadening has been proved to depend on the type of CH group and on the vibrational mode.

To interpret IR results quantitatively, the local CH environment and disorder have been considered. The bandwidth and line shift have been explained through a microstructural model taking into account screening effects and local disorder: CH_2 and CH_3 stretching widths have been proved to be very sensitive to disorder. The determination of H distribution in the film has shown that H is preferentially attached to sp^3 carbon. The evolution of the different effective charges has indicated that *a*-C:H microstructure is strongly heterogeneous and may rather be represented as a mixture at the atomic scale of hydrogenated C═C and C—C bonds interconnected to form the sp^2/sp^3 carbon network.

ACKNOWLEDGMENT

The authors are grateful to C. Clerc for RBS/ERD measurements.

*Author to whom correspondence should be addressed. FAX: 1-69-33-30-06. Electronic address: heitz@poly.polytechnique.fr

[1] J. Robertson, Surf. Coat. Technol. **50**, 185 (1992).
[2] Y. Hamakawa, T. Toyama, and H. Okamoto, J. Non-Cryst. Solids **115**, 180 (1989).
[3] C. Jäger, J. Gottwald, H. W. Spiess, and R. J. Newport, Phys. Rev. B **50**, 846 (1994).
[4] J. J. Cuomo, J. P. Doyle, J. Bruley, and J. C. Liu, J. Vac. Sci. Technol. A **9**, 2210 (1991).
[5] T. Heitz and B. Drévillon, Thin Solid Films **313–314**, 704 (1998).
[6] C. De Martino, F. Demichelis, and A. Tagliaferro, Diamond Relat. Mater. **4**, 1210 (1995).
[7] P. Couderc and Y. Catherine, Thin Solid Films **146**, 93 (1987).
[8] A. Grill and V. Patel, Appl. Phys. Lett. **60**, 2089 (1992).
[9] L. Martinu, A. Raveh, D. Boutard, S. Houle, D. Poitras, N. Vella, and M. R. Wertheimer, Diamond Relat. Mater. **2**, 673 (1993).
[10] P. J. R. Honeybone, R. J. Newport, J. K. Walters, W. S. Howells, and J. Tomkinson, Phys. Rev. B **50**, 839 (1994).
[11] B. Dischler, in *Amorphous Hydrogenated Carbon Films*, EMRS Symposia Proceedings, Vol. 17, edited by P. Koidl and P. Oelhaven (Les Editions de Physique, Paris, 1987), p. 189.
[12] R. Stief, J. Schäfer, J. Ristein, L. Ley, and W. Beyer, J. Non-Cryst. Solids **198–200**, 636 (1996).
[13] W. Jacob and M. Unger, Appl. Phys. Lett. **68**, 475 (1996).
[14] M. H. Brodsky, M. Cardona, and J. J. Cuomo, Phys. Rev. B **38**, 2988 (1988).
[15] W. Jacob and W. Möller, Appl. Phys. Lett. **63**, 1771 (1993).
[16] J. J. Fox and A. E. Martin, Proc. R. Soc. London, Ser. A **175**, 208 (1940).
[17] A. S. Wexler, Spectrochim. Acta **21**, 1725 (1965).
[18] H. Shanks, C. J. Fang, L. Ley, M. Cardona, F. J. Demond, and S. Kalbitzer, Phys. Status Solidi B **100**, 43 (1980).
[19] A. A. Langford, M. L. Fleet, B. P. Nelson, W. A. Lanford, and N. Maley, Phys. Rev. B **45**, 13 367 (1992).
[20] S. Vallon, E. Compain, and B. Drévillon, Rev. Sci. Instrum. **66**, 3269 (1995).
[21] T. Heitz, B. Drévillon, J. E. Bourée, and C. Godet, Appl. Phys. Lett. **72**, 780 (1998).
[22] R. Etemadi, C. Godet, J. Perrin, B. Drévillon, J. Huc, J. Y. Parey, J. C. Rostaing, and F. Coeuret, J. Vac. Sci. Technol. A **15**, 320 (1997).
[23] V. Yakovlev, B. Drévillon, N. Layadi, and P. Roca i Cabarrocas, J. Appl. Phys. **74**, 2535 (1993).
[24] J. E. Bourée, C. Godet, B. Drévillon, R. Etemadi, T. Heitz, J. Cernogora, and J. L. Fave, J. Non-Cryst. Solids **198–200**, 623 (1996).
[25] J. E. Bourée, C. Godet, R. Etemadi, and B. Drévillon, Synth. Met. **76**, 191 (1996).
[26] A. R. Forouhi and I. Bloomer, Phys. Rev. B **34**, 7018 (1986).
[27] F. Demichelis, C. F. Pini, and A. Tagliaferro, Phys. Rev. B **45**, 14 364 (1992); see also Ref. 57.
[28] N. Blayo and B. Drévillon, Appl. Phys. Lett. **59**, 950 (1991).
[29] A. Canillas, E. Bertran, J. L. Andujar, and B. Drévillon, J. Appl. Phys. **68**, 2752 (1990).
[30] E. B. Wilson, J. C. Delcius, and P. C. Cross, *Molecular Vibrations* (McGraw-Hill, New York, 1955), p. 162.
[31] H. Ratajczak and W. J. Orville-Thomas, Trans. Faraday Soc. **61**, 2603 (1965).
[32] L. Onsager, J. Am. Chem. Soc. **58**, 1486 (1936).
[33] M. Cardona, Phys. Status Solidi B **118**, 463 (1983).
[34] R. Ossikovski and B. Drévillon, Phys. Rev. B **54**, 10 530 (1996).
[35] S. C. Decius, J. Mol. Spectrosc. **57**, 348 (1975).
[36] L. A. Gribov, *Intensity Theory for Infrared Spectra of Polyatomic Molecules* (Consultants Bureau, New York, 1964).
[37] C. Castiglioni, M. Gusoni, and G. Zerbi, J. Mol. Struct. **198**, 475 (1989).
[38] M. Gusoni, J. Mol. Struct. **141**, 63 (1986).
[39] M. Gusoni, J. Mol. Struct. **113**, 323 (1984).
[40] A. von Keudell and W. Jacob, J. Appl. Phys. **81**, 1531 (1997).
[41] R. N. Jones, Spectrochim. Acta **9**, 235 (1957).
[42] S. A. Francis, J. Chem. Phys. **18**, 861 (1950).
[43] A. S. Wexler, Appl. Spectrosc. Rev. **1**, 29 (1967).
[44] R. G. Snyder, J. Chem. Phys. **42**, 1744 (1965).
[45] J. Baker, *Hyperconjugation* (Clarendon, Oxford, 1952).
[46] L. J. Bellamy, *Infrared Spectra of Complex Molecules* (Methuen, London, 1968), pp. 34–56.
[47] C. N. R. Rao, *Chemical Applications of Infrared Spectroscopy* (Academic, New York, 1963), p. 159.
[48] J. Robertson, Prog. Solid State Chem. **21**, 279 (1991).
[49] P. J. R. Honeybone, R. J. Newport, W. S. Howells, J. Tomkinson, and P. J. Revell, Chem. Phys. Lett. **180**, 145 (1991).
[50] T. Heitz, Ph.D. thesis, Ecole Polytechnique, France, 1998.
[51] A. Friedl, W. Fukarek, A. Möller, and A. Koch, Rev. Sci. Instrum. **65**, 2882 (1994).
[52] Y. Bounouh, M. L. Theye, A. Dehbi-Alaoui, A. Matthews, and J. P. Stoquert, Phys. Rev. B **51**, 9597 (1995).
[53] Y. Chabal, Surf. Sci. Rep. **8**, 213 (1988).
[54] A. M. Stoneham, Rev. Mod. Phys. **41**, 82 (1969).
[55] G. D. Mahan and A. A. Lucas, J. Chem. Phys. **68**, 1344 (1978).
[56] B. N. J. Person and R. Ryberg, Phys. Rev. B **24**, 6954 (1981).
[57] J. C. Angus and F. Jansen, J. Vac. Sci. Technol. A **6**, 1778 (1988).
[58] M. Weiler, S. Sattel, T. Giessen, K. Jung, H. Ehrhardt, V. S.

Veerasamy, and J. Robertson, Phys. Rev. B **53**, 1594 (1996).
[59] W. Burns, M. A. McKervey, T. R. Mitchell, and J. J. Rooney, J. Am. Chem. Soc. **100**, 906 (1978).
[60] C. Godet, T. Heitz, J. E. Bourée, B. Drévillon, and C. Clerc, J. Appl. Phys. (to be published).
[61] J. W. Zou, K. Reichelt, K. Schmidt, and B. Dischler, J. Appl. Phys. **65**, 3914 (1989).
[62] A. Friedel, W. Fukarek, W. Möller, and A. Koch, Rev. Sci. Instrum. **65**, 2882 (1994).
[63] See Refs. 21 and 57.
[64] D. R. McKenzie, R. C. McPhedran, N. Savvides, and L. C. Botton, Philos. Mag. B **48**, 341 (1983).
[65] J. Robertson and E. P. O'Reilly, Phys. Rev. B **35**, 2946 (1987).
[66] N. B. Colthup, L. H. Daly, and S. E. Wiberley, *Introduction to Infrared and Raman Spectroscopy* (Academic, Boston, 1990).
[67] H. Luther and G. Czerwony, Z. Phys. Chem., Neue Folge **6**, 286 (1956).